communications chemistry

A Nature Portfolio journal

Article

https://doi.org/10.1038/s42004-026-02141-0

Inorganic benzenes with inverted singlet-triplet gaps

Check for updates

Katsuyuki Shizu[1], Kuraudo Ishihara[1], Hiroki Uratani[2] & Hironori Kaji[1]

Inorganic-type benzenes have attracted significant attention due to their unique physical and chemical properties that are different from organic benzene. In this study, we theoretically investigate the possibility of inorganic benzenes as wide-gap materials with inverted singlet and triplet (iST) excited states. Since iST materials are expected to allow extremely efficient triplet to singlet conversion, they are promising as fluorescent and assist dopant materials for light-emitting diodes. From theoretical calculations, borazine ($B_3N_3H_6$), one of the most well-known inorganic benzenes, and its derivatives are expected not only to show iST but also to exhibit fast radiative decays surpassing those of typical iST materials: azaphenalene derivatives. Borthiin ($B_3S_3H_3$), boroselenol ($B_3Se_3H_3$), and the gallium-nitride analogue of benzene ($Ga_3N_3H_6$) are also expected to show iST with wide optical gaps.

Inorganic-type benzenes are six-membered six-π-electron systems having electronic structures analogous to organic benzene (hereafter referred to simply as benzene as usual)[1]. Borazine ($B_3N_3H_6$) is one of the most representative inorganic benzenes, consisting of alternating boron (B) and nitrogen (N) atoms arranged in a hexagonal ring (Fig. 1a)[2]. While numerous materials exhibiting visible to near-infrared emission have been widely explored for organic light-emitting diodes (OLEDs), those with ultraviolet (UV) to deep-UV (DUV) emission for OLEDs remain underdeveloped, despite their broad potential across wide variety of applications[3]. Hexagonal boron nitride (hBN), a structural analog of graphene, is known to be a semiconductor that shows a wide optical band gap and is promising as a UV to DUV emitter in optoelectronic applications[4,5]. Boron nitride nanotubes (BNNTs)[6], structural analogs of carbon nanotubes, also show wide band gaps suitable for such applications[7]. Recent advances in the synthesis makes it possible to develop diverse inorganic benzenes, including boron-nitride-based compounds consisting of four-B and two-N atoms[8] ($B_4N_2R_2R'_2R''_2$), boroxine[9] ($B_3O_3H_3$), borthiin[10] ($B_3S_3R_3$), boroselenol[11] ($B_3Se_3R_3$), phosphaborazine[12] ($B_3P_3R_3R'_3$), phosphazene[13] ($N_3P_3R_6$) and its gallium analog[14] ($Ga_3P_3R_3R'_3$), aluminum analog (alumazene[15]; $Al_3N_3R_3R'_3$) and its phosphor and arsenic analogs[16] ($Al_3P_3R_3R'_3$ and $Al_3As_3R_3R'_3$, respectively), as well as triphospha- and triarsa-trisilabenzenes[17] ($Si_3P_3R_3$ and $Si_3As_3R_3$, respectively), and the germanium analog (germanazene[18]; $Ge_3N_3R_3$), where R, R', and R" denote substituents. The structural diversity of these inorganic benzenes allows us to develop novel materials with unique photophysical properties that are unattainable in conventional carbon-based aromatic systems.

The doubly degenerate highest occupied molecular orbital (HOMO) and lowest unoccupied molecular orbital (LUMO) of borazine are predominantly localized on the N and B atoms, respectively (Fig. 1b). Thus, the HOMO→LUMO excitation of borazine can be viewed as the short-range charge-transfer[19] (SRCT) electronic excitation between the N and B atoms. For the inorganic-type benzenes listed above, S_1 can be energetically lower than T_1 as confirmed below, leading to a unique electronic property called the inverted singlet-triplet (iST or INVEST): the S_1-T_1 energy difference ΔE_{ST} is negative. Here, $\Delta E_{ST} = E(S_1) - E(T_1)$; $E(S_1)$ and $E(T_1)$ are the S_1 and T_1 energies, respectively.

The presence of iST was originally suggested theoretically by Borden[20], Kollmar, and Staemmler[21] for cyclobutadiene in the 1970s. Experimental iST study was performed by Leupin and Wirz for cycl[3.3.3]azine[22] in 1980. After a long silence, interest in iST was reignited by a pivotal theoretical study by de Silva in 2019, which clearly demonstrated the possibility of negative singlet-triplet gap by considering double excitations[23]. Experimental observations have also emerged for azaphenalene derivatives, following the work by Domcke's group in 2019[24–28]. These works have further driven theoretical efforts toward accurate estimation of singlet-triplet energy gaps, where high-order excitations play an important role[29–32]. Because iST allows a thermodynamically favorable $T_1 \rightarrow S_1$ transition, iST materials can show efficient reverse intersystem crossing (RISC) from T_1 to S_1 and are promising as fluorescent materials for organic light-emitting diodes (OLEDs). However, to date, the rate constants for $S_1 \rightarrow S_0$ fluorescence (k_F) are not large enough, on the order of 10^6 s^{-1}. In this study, we theoretically investigate the potential iST character of inorganic benzenes. Our quantum chemical calculations indicate that borazine derivatives are promising candidates for electroluminescent UV emitters exhibiting both negative ΔE_{ST} and k_F of 10^7–10^8 s^{-1} (see Table 1 below). These k_F values, one to two orders of magnitude higher than those of previously reported iST molecules, represent a significant advancement in emitter performance. Borthiins and boroselenol are also found to show negative ΔE_{ST} and are candidates for core

[1]Institute for Chemical Research, Kyoto University, Uji, Kyoto, Japan. [2]Department of Molecular Engineering, Graduate School of Engineering, Kyoto University, Kyoto, Japan. e-mail: kaji@scl.kyoto-u.ac.jp

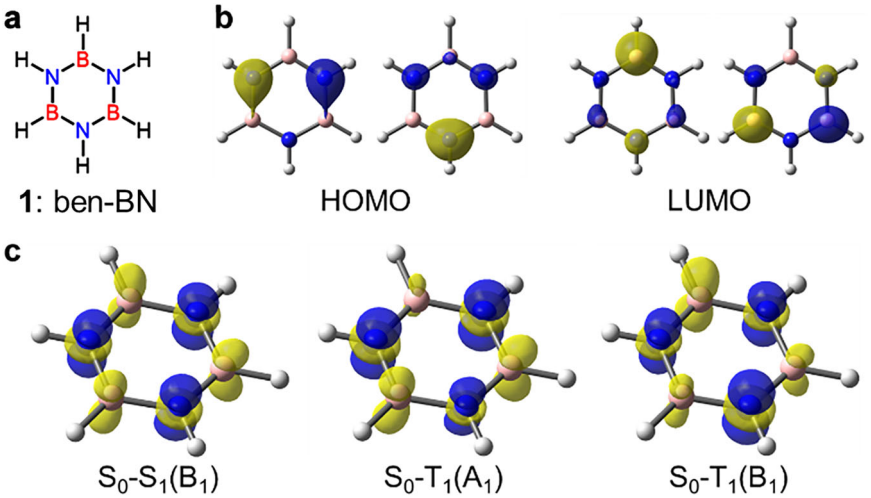

Fig. 1 | Short-range charge-transfer electronic excitations in borazine. a Chemical structure of borazine (**1:** benzene-type boron nitride, **ben-BN**). **b** Frontier orbitals of **1: ben-BN** calculated at the HF/cc-pVTZ//PBE0/6-31G(d) level of the theory. Two MOs are degenerate in both HOMO and LUMO. **c** Electron-density difference ($\Delta\rho$) maps arising from the $S_0 \rightarrow S_1(B_1)$, $S_0 \rightarrow T_1(A_1)$, and $S_0 \rightarrow T_1(B_1)$ excitations in **1: ben-BN**. Here, $T_1(A_1)$ and $T_1(B_1)$ represent doubly degenerate T_1 of different symmetries, A_1 and B_1, respectively. Blue regions show negative $\Delta\rho$, where the electron density decreases. Yellow regions show positive $\Delta\rho$, where the electron density increases.

Table 1 | Point groups and ΔE_{ST}, $E(S_1)$, $E(T_1)$, μ_F, f, k_F, k_{ISC}, and k_{RISC} of inorganic benzenes calculated with the SCS-CC2/def2-TZVP//PBE0/6-31G(d) method

	Molecular formula	Point group	ΔE_{ST} (meV)	$E(S_1)$ (eV)	$E(T_1)$ (eV)	μ_F (au)	f	k_F (s^{-1})	k_{ISC} (s^{-1})	k_{RISC} (s^{-1})
1: ben-BN	$B_3N_3H_6$	D_{3h}	**−295**	6.83	7.13	0.0000	0.0	0.0	4.5×10^2	$\mathbf{1.5 \times 10^7}$
2a: naph-BN	$B_5N_5H_8$	C_{2v}	**−95**	6.64	6.73	0.1502	3.7×10^{-3}	7.0×10^6	2.4×10^6	$\mathbf{3.4 \times 10^7}$
2b: anth-BN	$B_7N_7H_{10}$	C_{2v}	**−21**	6.63	6.65	0.4159	2.8×10^{-2}	$\mathbf{5.4 \times 10^7}$	0.0	0.0
2c: phenan-BN	$B_7N_7H_{10}$	C_s	**−127**	6.57	6.70	0.2990	1.4×10^{-2}	$\mathbf{2.7 \times 10^7}$	2.8×10^5	$\mathbf{1.9 \times 10^7}$
2d: tetra-BN	$B_9N_9H_{12}$	C_{2v}	**−51**	6.62	6.67	0.7023	8.0×10^{-2}	$\mathbf{1.5 \times 10^8}$	0.0	0.0
2e: cryc-BN	$B_9N_9H_{12}$	C_s	**−59**	6.56	6.62	0.1300	2.7×10^{-3}	5.1×10^6	4.7×10^6	$\mathbf{2.3 \times 10^7}$
2f: pyr-BN	$B_8N_8H_{10}$	C_{2v}	**−221**	6.54	6.76	0.0562	5.1×10^{-4}	9.4×10^5	2.5×10^3	$\mathbf{8.0 \times 10^6}$
2g: phenal-NB	$B_7N_6H_9$	D_{3h}	**−260**	6.59	6.85	0.0000	0.0	0.0	5.8×10^2	$\mathbf{5.4 \times 10^6}$
2h: phenal-BN	$B_6N_7H_9$	D_{3h}	**−128**	6.54	6.67	0.0000	0.0	0.0	0.0	0.0
2i: olymp-NB	$B_{10}N_9H_{11}$	C_{2v}	**−243**	6.54	6.78	0.0284	1.3×10^{-4}	2.4×10^5	0.0	0.0
2j: olymp-BN	$B_9N_{10}H_{11}$	C_{2v}	**−97**	6.53	6.63	0.2545	1.0×10^{-2}	$\mathbf{1.9 \times 10^7}$	0.0	0.0
2k: bis-BN	$B_{14}N_{14}H_{14}$	C_{2v}	**−57**	6.54	6.59	0.2110	7.1×10^{-3}	$\mathbf{1.3 \times 10^7}$	0.0	0.0
3: (6, 6)NB-BN	$B_{24}N_{24}H_{24}$	S_6	**−141**	6.26	6.40	0.0000	0.0	0.0	6.1×10^3	$\mathbf{1.4 \times 10^6}$
4e: [6]CPP-BN	$B_{18}N_{18}H_{24}$	S_6	**−145**	6.26	6.40	0.0000	0.0	0.0	6.7×10^2	1.2×10^5
5: [6]CMP-BN	$B_{18}N_{18}H_{24}$	C_{3v}	**−186**	6.45	6.64	0.0000	0.0	0.0	1.4×10^2	7.6×10^4
6e: [6]PP-BN	$B_{18}N_{18}H_{26}$	C_2	**−77**	6.58	6.66	0.0458	3.4×10^{-4}	6.4×10^5	3.1×10^2	1.5×10^3
7f: [6]MP-BN	$B_{18}N_{18}H_{26}$	C_1	**−214**	6.49	6.70	0.0772	9.5×10^{-4}	1.7×10^6	1.0×10^3	$\mathbf{1.4 \times 10^6}$
8a: $B_{12}N_{12}$-fullerene	$B_{12}N_{12}$	T_h	**−134**	6.47	6.60	0.0000	0.0	0.0	6.6×10^1	3.8×10^3
9: ben-BS	$B_3S_3H_3$	D_{3h}	**−109**	5.02	5.13	0.0000	0.0	0.0	3.7×10^6	$\mathbf{1.8 \times 10^8}$
10: ben-BSe	$B_3Se_3H_3$	D_{3h}	**−160**	4.42	4.58	0.0000	0.0	0.0	1.2×10^7	$\mathbf{2.1 \times 10^9}$
11: ben-BO	$B_3O_3H_3$	D_{3h}	326	8.11	7.79	0.0000	0.0	0.0	6.3×10^{10}	1.6×10^5
12: ben-GaN	$Ga_3N_3H_6$	D_{3h}	**−230**	5.52	5.75	0.0000	0.0	0.0	0.0	0.0
13: prism-GaN	$Ga_3N_3H_6$	C_s	507	4.11	3.61	0.7097	5.1×10^{-2}	$\mathbf{3.7 \times 10^7}$	2.0×10^8	2.5×10^{-1}

units to develop wide gap iST materials for OLEDs. The gallium-nitride (GaN) analog of benzene ($Ga_3N_3H_6$) is also predicted to show iST character with a wide optical gap.

Results

Inorganic benzenes

Figures 1 and 2 show the structures and abbreviated names of the borazine family investigated in this study: borazine (**1: ben-BN**) and one- and two-dimensional (1D and 2D) fused borazines (**2a: naph-BN** to **2k: bis-BN**). In Fig. 2, the H atoms are omitted for clarity; the optimized structures with H atoms are shown in Supplementary Information (Supplementary Fig. 1). **2k: bis-BN** can be viewed as a model of hBN. ΔE_{ST}, $E(S_1)$, $E(T_1)$, the S_0-S_1 transition dipole moment (μ_F), the S_0-S_1 oscillator strength (f), and the rate constants k_F, the intersystem crossing rate constants (k_{ISC}), and the reverse intersystem crossing rate constants (k_{RISC}) of these compounds calculated with spin-component scaled second-order approximate coupled-cluster (SCS-CC2) are listed in Table 1. The detailed formulas used to evaluate the rate constants are presented in Supplementary Methods. These values were calculated at the S_0-optimized geometry at the PBE0/6-31G(d) level of theory. The corresponding data calculated with the second-order algebraic diagrammatic construction (ADC(2)) are listed in Supplementary Table 1, and the SCS-CC2 results at the geometries optimized at the MP2/6-31 G(d)

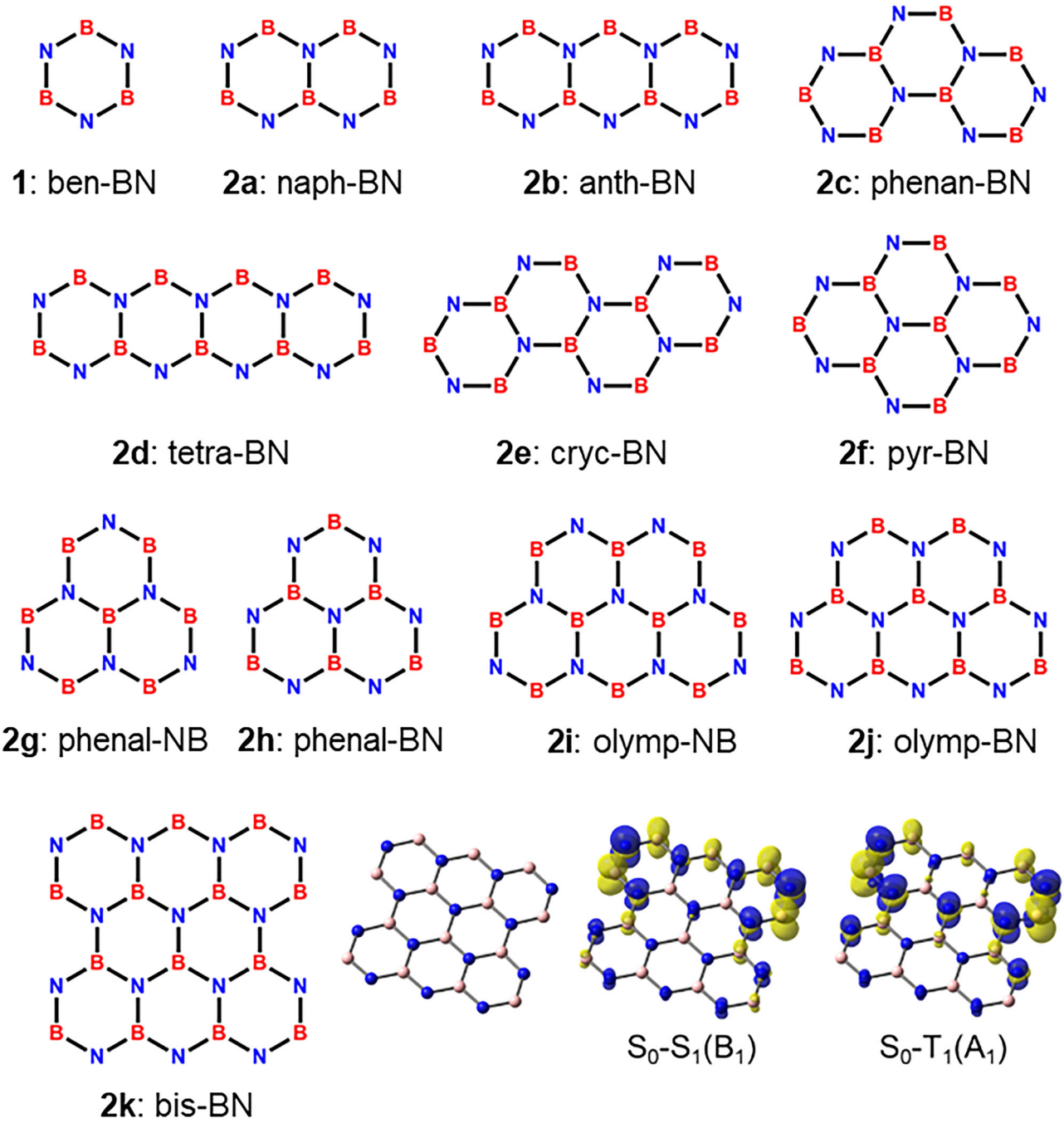

Fig. 2 | Schematic structures of borazine and one- and two-dimensional fused borazines. Hydrogen atoms are omitted for clarity. **1:** borazine (**ben-BN**), **2a:** naphthalene-type BN (**naph-BN**), **2b:** anthracene-type BN (**anth-BN**), **2c:** phenanthrene-type BN (**phenan-BN**), **2d: tetracene**-type BN (**tetra-BN**), **2e:** crycene-type BN (**cryc-BN**), **2f:** pyrene-type BN (**pyr-BN**), **2g:** phenalene-type nitride boron (**phenal-NB**), **2h:** phenalene-type BN (**phenal-BN**), **2i:** olympicene-type NB (**olymp-NB**), **2j:** olympicene-type BN (**olymp-BN**), and **2k:** bisanthrene-type BN (**bis-BN**). Electron-density difference ($\Delta\rho$) maps arising from the $S_0 \rightarrow S_1(B_1)$ and $S_0 \rightarrow T_1(A_1)$ excitations of **2k: bis-BN** are also shown. Blue regions show negative $\Delta\rho$ (where the electron density decreases). Yellow regions show positive $\Delta\rho$ (where the electron density increases).

level are listed in Supplementary Table 4. See the "Methods" section for the calculation details. Importantly, all of **1**: **ben-BN** to **2k: bis-BN** show negative ΔE_{ST} (<−21 meV) and large $E(S_1)$ (>6.53 eV), suggesting that these compounds are promising as wide-gap core materials with iST character. It would be possible to develop materials with preferred emission wavelengths through appropriate structural modifications. It is instructive to compare the present result for **1: ben-BN** with the previous report by Sobolewski and Domcke[33], in which calculated values of ΔE_{ST} for **1: ben-BN** were compared among several wavefunction-based methods. Their ADC(2)/cc-pVTZ result (ΔE_{ST} = −195 meV) is well reproduced by our ADC(2)/def2-TZVP calculation (ΔE_{ST} = −193 meV), where the slight deviation is attributed to the different optimization methods used for the reference geometry. They also reported that CC2/cc-pVTZ results in a less negative value (ΔE_{ST} = −90 meV), and EOM-CCSD/cc-pVTZ predicts a positive value (ΔE_{ST} = +19 meV). Compared to their results and our ADC(2)/def2-TZVP result, our SCS-CC2/def2-TZVP result (ΔE_{ST} = −295 meV) is considerably more negative. At this stage, it is difficult to judge which value is closest to the "exact" result due to the lack of experimental benchmarks. For the

calculations, more reliable reference values obtained with higher-order correlation treatments may be required. Sobolewski and Domcke also reported that ΔE_{ST} shifts positively (but still remains negative for the ADC(2) and CC2 methods) when cc-pVDZ basis set is used instead of cc-pVTZ. In view of this report, we also performed calculations with cc-pVDZ basis set for all the molecules considered in Table 1 (Supplementary Tables 6–8), indicating that the difference in the ΔE_{ST} values from the corresponding cc-pVTZ results does not substantially affect our discussion; the only one exception is **6e: [6]PP-BN**, for which the sign of ΔE_{ST} changes.

To confirm the SRCT character of **1**: **ben-BN**, we calculated electron-density difference ($\Delta\rho$) maps arising from the $S_0 \rightarrow S_1$ and $S_0 \rightarrow T_1$ excitations (Fig. 1c). The $\Delta\rho$ maps were calculated by subtracting the total electron density of S_0 from that of S_1 or T_1, using the S_0 structure. Figure 1c shows the $\Delta\rho$ maps for the $S_0 \rightarrow S_1(B_1)$, $S_0 \rightarrow T_1(A_1)$, and $S_0 \rightarrow T_1(B_1)$ excitations of **1: ben-BN**, where $T_1(A_1)$ and $T_1(B_1)$ represent doubly degenerate T_1 of different symmetries, A_1 and B_1, respectively. Blue regions show negative $\Delta\rho$, where the electron density decreases, and yellow regions show positive $\Delta\rho$, where the electron density increases. The negative $\Delta\rho$ is strongly localized on the N atoms, whereas the positive $\Delta\rho$ is strongly localized on the B atoms, suggesting that a short-range electron transfer from the N to B atoms occurs upon the excitations. In addition, $\Delta\rho$ shows spatially alternating negative and positive regions, which are characteristic for B- and N-containing molecules with small positive ΔE_{ST}[34–36] and heptazine derivatives with negative ΔE_{ST}[37]. Fig. 2 shows calculated $\Delta\rho$ maps for the $S_0 \rightarrow S_1(B_1)$ and $S_0 \rightarrow T_1(A_1)$ excitations of **2k: bis-BN**. Like **1**: **ben-BN, 2k: bis-BN** has spatially alternating negative and positive regions, indicating SRCT character.

From Eqs. (S1) and (S2) in the Supplementary Information, a large μ_F is desirable to increase f and k_F, which enhances the luminescence efficiency. From Table 1, it is found that f is large for 1D structures, especially when the fused ring becomes longer (**1: ben-BN→2a: naph-BN→2b: anth-BN→2d: tetra-BN**), whereas it vanishes when the molecular structure is 3-fold triangular symmetric (**1**: **ben-BN, 2g**: **phenal-NB**, and **2h**: **phenal-BN**). **2d**: **tetra-BN** shows the largest k_F of 1.5×10^8 s^{-1} among the molecules in Fig. 2. These results suggest that breaking the C_3 symmetry and extending the molecular framework in one direction are key factors for increasing μ_F, f, and the resulting k_F. Table 1 also shows k_{ISC} and k_{RISC} between S_1 and T_1. It has been reported that activation barriers can exist in RISC processes even when ΔE_{ST} is negative[38,39]. Further, quantitative estimation of rate constants requires nuclear quantum effects to be taken into account. We therefore employed analytical expressions for k_{ISC} and k_{RISC} derived via Fermi's golden rule with explicit consideration of nuclear quantum effects[40,41], as summarized in the Supplementary Method. For molecules with large k_F (>10^7 s^{-1}), k_{ISC} was smaller by orders of magnitude, except for **13: prism-GaN**. This result suggests that ISC is unlikely to compete with fluorescence. The calculated k_{RISC} values indicate that **1: ben-BN, 2a: naph-BN, 2c: phenan-BN, 2e: cryc-BN, 2f: pyr-BN, 2**g: phenal-BN, **3: (6, 6)NB-BN, 7f: [6]MP-BN, 9: ben-BS**, and **10: ben-BSe** have RISC rate constants over 10^6 s^{-1}, which are comparable to typical values reported for known TADF emitters. In comparison with the SCS-CC2 results (Table 1), the ADC(2) results (Supplementary Table 1) tend to yield less negative ΔE_{ST} values, while the sign remains unchanged for majority of the molecules.

To evaluate the performance as emitters in more detail, we also performed calculations at S_1-optimized geometries. In addition to k_F, k_{ISC}, and k_{RISC}, the nonradiative decay rate constants (k_{NR}) were also calculated. The results (Supplementary Table 5) indicate that k_{NR} and k_{ISC} are smaller than k_F for molecules with large k_F (>10^8 s^{-1}), suggesting that fluorescence is the dominant relaxation pathway from S_1 in these molecules.

Ring- and fullerene-type borazines

Figure 3 shows cyclic borazines, which are parts of BNNTs. The ΔE_{ST}, $E(S_1)$, μ_F, f, and k_F values are also shown in Table 1. **3: (6, 6)NB-BN** is a subunit of a BNNT, consisting of 12 fused borazine rings. The structure of **3: (6, 6)NB-BN** was designed with reference to a carbon nanobelt structure in ref. 42. (a subunit of a (6, 6)-carbon nanotube) and then, optimized at the PBE0/6-31 G(d) level of theory. **3: (6, 6)NB-BN** shows a negative ΔE_{ST} of −141 meV and a large $E(S_1)$ of 6.26 eV (Table 1). Figure 3 also shows the calculated $\Delta\rho$ maps for the $S_0 \rightarrow S_1(A_g)$ and $S_0 \rightarrow T_1(A_g)$ excitations of **3: (6, 6)NB-BN**. Similarly to the above cases, the negative $\Delta\rho$ (blue regions) is strongly localized on the N atoms, whereas the positive $\Delta\rho$ (yellow regions) is strongly localized on the B atoms, suggesting that S_1 and T_1 of **3: (6, 6)NB-BN** also have pure SRCT character. The f value of **3: (6, 6)NB-BN** vanishes because of the symmetric ring structure, which would make **3: (6, 6)NB-BN** non-emissive. **4e: [6]CPP-BN** is another subunit of the BNNT; the diameter of **4e: [6]CPP-BN** (8.36 Å) is slightly larger than that of **3: (6, 6)NB-BN** (8.32 Å). **4e: [6]CPP-BN** consists of six borazine rings and is the borazine analog of [6]cycloparaphenylene ([6]CPP)[43], a subunit of a (6,6)-carbon nanotube. The ΔE_{ST}, $E(S_1)$, μ_F, f, and k_F of **4e: [6]CPP-BN** are similar to those of **3: (6, 6)NB-BN**, despite the difference in conjugated state. **5**: **[6]CMP-BN** also consists of six borazine rings but forms a different ring configuration; the borazine analog of [6]cyclometaphenylene[44]. The ΔE_{ST} of **5: [6]CMP-BN** (−186 meV) is smaller than those of **3: (6, 6)NB-BN** and **4e: [6]CPP-BN**. Similarly to **3: (6, 6)NB-BN** and **4e: [6]CPP-BN**, the symmetric ring structure results in $f = 0$. To understand the influence of the ring structures on the f values, we compared the f values of **4e: [6]CPP-BN** and **5: [6]CMP-BN** with those of their 1D counterparts, **6e: [6]PP-BN** and **7f: [6]MP-BN**. Unlike **4e: [6]CPP-BN** and **5: [6]CMP-BN, 6e: [6]PP-BN** and 7f: [6]MP-BN have non-zero f values, leading to k_F of the order of 10^5–10^6 s^{-1}, suggesting that the symmetric ring formation largely decreases f value. The calculated ΔE_{ST}, $E(S_1)$, μ_F, f, and k_F values for 5–12-membered borazine rings and their 1D counterparts are summarized in Supplementary Information (molecules **4d: [5]CPP-BN** - **4k**: **[12]CPP-BN** in Supplementary Fig. 2, molecules **6a: [2]PP-BN** - **6k: [12]PP-BN** in Supplementary Fig. 3, and Supplementary Table 2). The ring molecules (**4d: [5]CPP-BN** - **4k**: **[12]CPP-BN**) have zero or nearly zero f values, whereas the 1D counterparts (**6d: [5]PP-BN** - **6h: [9]PP-BN**) have non-zero f values with k_F of 10^4–10^6 s^{-1}. Linear metaphenylene-type molecules (**7a: [3]MP-BN** - **7f: [6]MP-BN**) also have non-zero f values with k_F of 10^5–10^7 s^{-1} (Supplementary Fig. 4 and Supplementary Table 2).

Borazine analogs of fullerenes have been experimentally observed[45–47]. $B_{12}N_{12}$-fullerene is a borazine analog of C_{24} fullerene and consists of the four- and six-membered rings (note that **8a: $B_{12}N_{12}$-fullerene** and all fullerene-type compounds have no H atoms). **8a: $B_{12}N_{12}$-fullerene** shows a negative ΔE_{ST} of −134 meV, which is comparable to those of **3: (6, 6)NB-BN** and **4e: [6]CPP-BN** (−141 and −145 meV, respectively). S_1 and T_1 of **8a: $B_{12}N_{12}$-fullerene** are triply degenerate (denoted as A_2, B_1, and B_2) owing to its highly symmetric structure. Figure 3 shows $\Delta\rho$ maps for the $S_0 \rightarrow S_1$ and $S_0 \rightarrow T_1$ excitations of **8a: $B_{12}N_{12}$-fullerene**. The negative and positive $\Delta\rho$ distributions suggest that S_1 and T_1 of **8a: $B_{12}N_{12}$-fullerene** show pure SRCT character. Like the ring borazines of **3: (6, 6)NB-BN, 4e: [6]CPP-BN**, and **5: [6]CMP-BN, 8a: $B_{12}N_{12}$-fullerene** has zero f value and is expected to be non-emissive. The calculated results for borazine analogs of C_{48} and C_{72} fullerenes are shown in Supplementary Information (molecules **8b: $B_{24}N_{24}$-fullerene** and **8c: $B_{36}N_{36}$-fullerene** in Supplementary Fig. 5 and Supplementary Table 2). Although **8b: $B_{24}N_{24}$-fullerene** and **8c: $B_{36}N_{36}$-fullerene** show positive ΔE_{ST}, the ΔE_{ST} values (~k_BT at room temperature) are sufficiently small to induce rapid $T_1 \rightarrow S_1$ transition.

Inorganic-type benzenes other than borazine

Finally, we investigate the potential of inorganic-type benzenes other than borazine-based compounds as wide-gap iST materials (**9: ben-BS** - **13: prism-GaN** in Fig. 4 and **14: ben-B_4N_2** - **23: ring-Ge_3N_3** in Supplementary Fig. 6). Derivatives of **9: ben-BS** - **11: ben-BO** and **14: ben-B_4N_2** - **23: ring-Ge_3N_3** have been experimentally synthesized[8–18], whereas **12**: **ben-GaN** and **13: prism-GaN** have been only theoretically predicted[48,49]. Substituents required for organic synthesis are replaced with H atoms. Borthiin (**9: ben-BS**) and boroselenol (**10: ben-BSe**) show negative ΔE_{ST} (<−100 meV), whereas the oxygen (O) analog (boroxine, **11: ben-BO**) shows a large positive ΔE_{ST} of 326 meV (Table 1). To understand the difference in the ΔE_{ST} values of **9: ben-BS** - **11: ben-BO**,

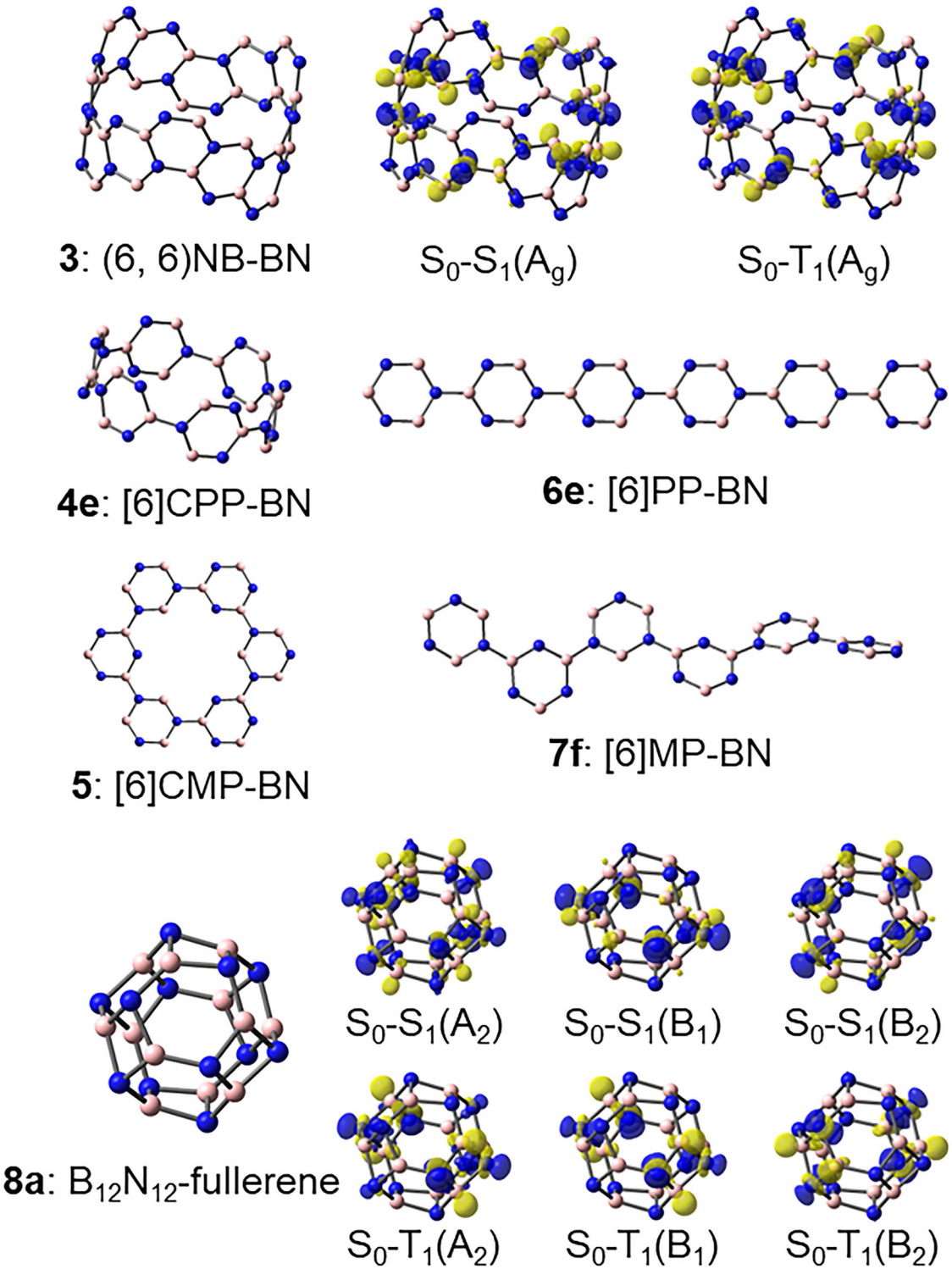

Fig. 3 | DFT-optimized structures of ring-type borazines (3, 4e, and 5), their one-dimensional counterparts (6e and 7f), and a fullerene-type BN compound (8a) at the PBE0/6-31G(d) level of theory. 3: (6, 6)carbon nanobelt-type BN (**(6, 6)NB-BN**), **4e:** [6]cycloparaphenylene-type BN (**[6]CPP-BN**), **6e:** [6]paraphenylene-type BN (**[6]PP-BN**), **5:** [6]cyclometaphenylene-type BN (**[6]CMP-BN**), **7f:** [6]meta-phenylene-type BN (**[6]MP-BN**), **8a:** C_{24}-fullerene-type BN (**$B_{12}N_{12}$-fullerene**). Hydrogen atoms are omitted for clarity except for **8a: $B_{12}N_{12}$-fullerene**. Electron-density difference ($\Delta\rho$) maps arising from the $S_0 \rightarrow S_1(A_g)$ and $S_0 \rightarrow T_1(A_g)$ excitations of **3: (6, 6)NB-BN** and the $S_0 \rightarrow S_1(A_2)$, $S_0 \rightarrow S_1(B_1)$, $S_0 \rightarrow S_1(B_2)$, $S_0 \rightarrow T_1(A_2)$, $S_0 \rightarrow T_1(B_1)$, and $S_0 \rightarrow T_1(B_2)$ excitations of **8a: $B_{12}N_{12}$-fullerene** are also shown. Blue regions show negative $\Delta\rho$ (where the electron density decreases). Yellow regions show positive $\Delta\rho$ (where the electron density increases). The twisted structure is most stable for **7f: [6]MP-BN**, due to the steric hindrance among H atoms.

we compared the $\Delta\rho$ maps for the $S_0 \rightarrow S_1$ and $S_0 \rightarrow T_1$ excitations of **9: ben-BS** - **11: ben-BO** (Fig. 4). For **9: ben-BS** and **10: ben-BSe**, the negative $\Delta\rho$ is strongly localized on the S and Se atoms, whereas the positive $\Delta\rho$ is strongly localized on the B atoms. The $\Delta\rho$ patterns are similar to those observed for borazine (**1: ben-BN**, Fig. 1). Meanwhile, for **11: ben-BO**, the negative $\Delta\rho$ is largely distributed on the B-O and B-H bonds, whereas the positive $\Delta\rho$ is strongly localized on B atoms, which breaks down SRCT character. This pattern of $\Delta\rho$ suggests the significant

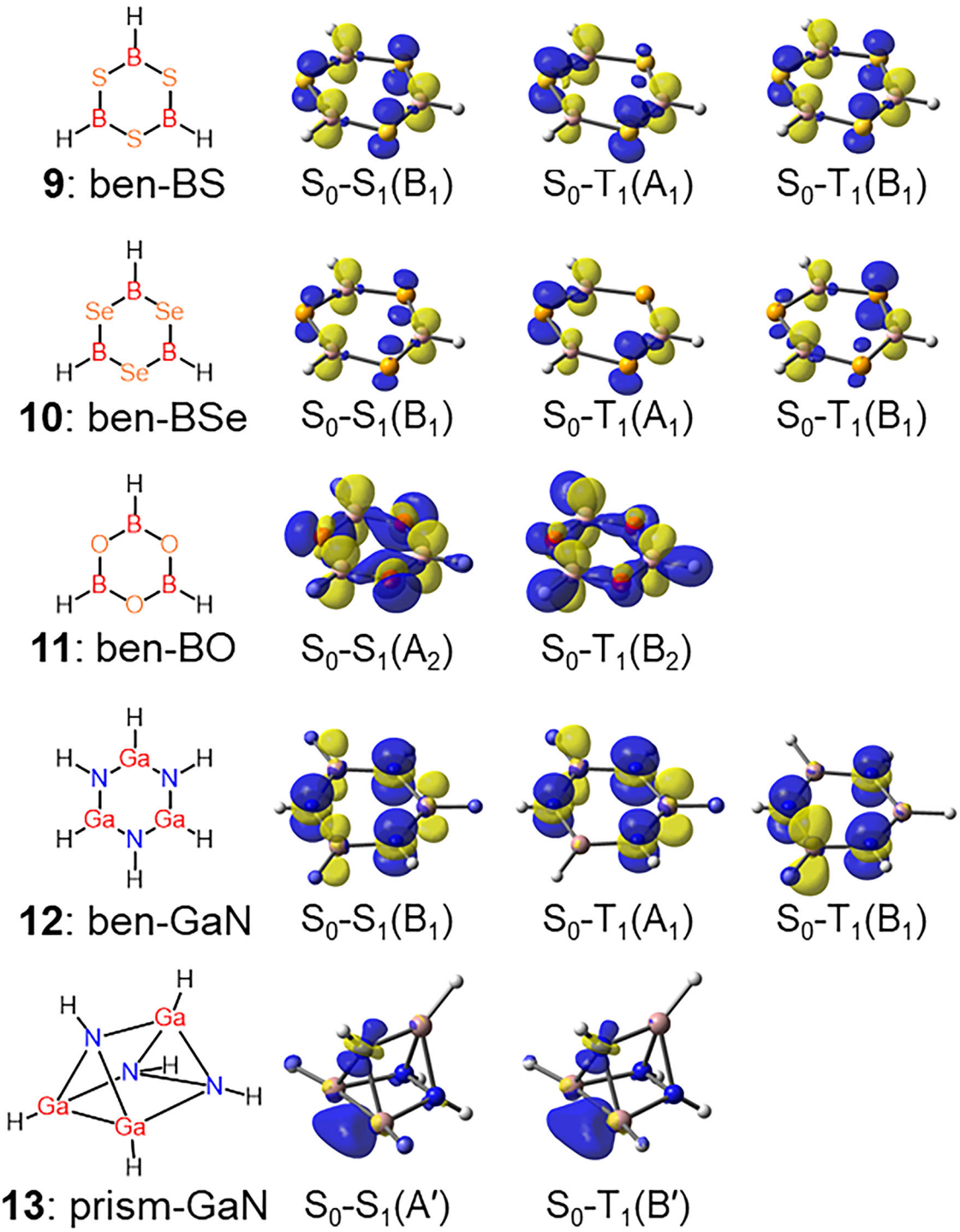

Fig. 4 | Inorganic-type benzenes other than borazine. 9: borthiin (benzene-type boron sulfide; **ben-BS**), **10:** boroselenol (benzene-type boron selenide; **ben-BSe**), **11:** boroxine (benzene-type BO; **ben-BO**), **12:** benzene-type gallium nitride (**ben-GaN**), **13:** prismane-type gallium nitride (**prism-GaN**). Electron-**density** difference ($\Delta\rho$) maps arising from the $S_0 \rightarrow S_1$ and $S_0 \rightarrow T_1$ excitations of **9: ben-BS** - **13**: **prism-GaN** are also shown. Blue regions show negative $\Delta\rho$, where the electron density decreases. Yellow regions show positive $\Delta\rho$, where the electron density increases.

overlap of the MOs, which may yield large exchange interaction that dominates over the spin polarization (double excitation) effect, leading to the large positive ΔE_{ST} of 326 meV. GaN is a wide-bandgap semiconductor and is widely used for blue and white light-emitting diodes[50–53]. Hence, although the GaN analog of benzene ($Ga_3N_3H_6$) has not been synthesized yet, it is worth investigating its potential iST property. Two structures have been theoretically proposed for $Ga_3N_3H_6$: a planar benzene-type structure[48] (**12: ben-GaN**), where Ga and N atoms are arranged alternatively, and a prismane-type structure[49] (**13: prism-GaN**), where two Ga and N atoms are adjacent to each other. Calculated $\Delta\rho$ maps for the $S_0 \rightarrow S_1$ and $S_0 \rightarrow T_1$ excitations of **12: ben-GaN** show SRCT with spatially alternating negative and positive regions, whereas those of **13: prism-GaN** have large distributions on the Ga-Ga bonds. Consequently, **12: ben-GaN** shows negative ΔE_{ST} of −230 meV, whereas **13: prism-GaN** shows a large positive ΔE_{ST} of 507 meV (Table 1). Thus, like borazine, the GaN analog of benzene (**12: ben-GaN**) is predicted to

show iST owing to its SRCT character in the $S_0 \rightarrow T_1$ and $S_0 \rightarrow S_1$ excitations. For other inorganic-type molecules, **14: ben-B_4N_2**, **15: ben-BP**, **16: ben-NP**, **17: ring-Ga_3P_3**, **18: ben-AlN**, **19: ring-Al_3P_3**, **20: ring-Al_3As_3**, **21: ring-$(Si(N_2CH_3))_3P_3$**, **22: ring-$(Si(N_2CH_3))_3As_3$**, and **23: ring-Ge_3N_3** (Supplementary Fig. 6), ΔE_{ST} were calculated to be positive (>100 meV, Supplementary Table 3). Among the 15 inorganic benzenes (**9: ben-BS** – **23: ring-Ge_3N_3**) examined in Fig. 4 and Supplementary Fig. 6, only **9: ben-BS**, **10: ben-BSe**, and **12: ben-GaN** were expected to show iST.

Discussion

We theoretically investigated the potential iST character of inorganic-type benzenes, mainly focusing on borazines. 2D-sheet, ring, and fullerene-type borazines showed the SRCT from N to B atoms in $S_0 \rightarrow S_1$ and $S_0 \rightarrow T_1$ excitations, which leads to the large inverted S_1 and T_1 energies. Other than borazines, ben-BS ($B_3S_3H_3$, borthiin), ben-BSe ($B_3Se_3H_3$, boroselenol), and the ben-GaN ($Ga_3N_3H_6$) were found to show iST. These molecules have large S_1 energies, leading to the development of promising electroluminescent UV emitters and wide-gap hosts with iST properties. Totally, we found 43 compounds with negative ΔE_{ST}s. Among them, several compounds exhibit k_F of 10^7–10^8 s^{-1}, which will be expected as efficient emitters. According to the present results, a limited number of molecules simultaneously satisfy sufficiently large k_F and k_{RISC}. Nevertheless, taking into account vibrational motion, exemplified by the Herzberg-Teller effect, might extend this compatibility to a larger number of molecules. In addition, by introducing various functional groups to these compounds, it is expected that excellent iST emitting materials with tunable emission wavelengths can be developed.

Methods

Geometry optimization

The ground-state (S_0) geometries of the inorganic-type benzene materials were optimized at the PBE0/6-31G(d) level of theory, and their singlet and triplet excited states were calculated using the SCS-CC2 method with the def2-TZVP basis for the S_0 geometries (the optimized geometries are listed in Supplementary Tables 9–65). The method is denoted as SCS-CC2/def2-TZVP//PBE0/6-31 G(d). For comparison, calculations were also performed for the MP2-optimized geometries, SCS-CC2/cc-pVTZ//MP2/6-31G(d) (Supplementary Table 4). Furthermore, calculations using the SCS-CC2/cc-pVTZ//TD-PBE0/6-31 G(d) method at the S_1 geometries were carried out (Supplementary Table 5). The SCS-CC2 method considers double-electron excitations and has been shown to accurately predict ΔE_{ST} for molecules consisting of B and N backbones[34–36]. The S_0- and S_1-geometry optimizations were performed using the Gaussian 16 program package[54].

Calculation of electronic properties

ΔE_{ST}, $E(S_1)$, $E(T_1)$, μ_F, and f were calculated using the Turbomole program package[55]. k_F, k_{ISC}, and k_{RISC} were calculated using Eqs. (S1)–(S5) in the Supplementary Information. The ADC(2) method also considers double-electron excitations and has been used to compute ΔE_{ST} of iST molecules[56]. The results for ADC(2) calculations are summarized in the Supplementary Information (Supplementary Tables 1–3). Note that triple excitations were not considered in this study due to the high computational cost (it has been reported that inclusion of triple excitations tends to make ΔE_{ST} less negative[29,57]). The S_1-T_1 spin-orbit coupling (SOC) values were estimated using PySOC package[58], based on the excited-state wavefunctions obtained at the TD-PBE0/6-31G(d) level of theory.

Data availability

All relevant data are available from the corresponding author (kaji@scl.kyoto-u.ac.jp) upon request.

Received: 8 December 2025; Accepted: 9 July 2026;
Published online: 18 July 2026

References

1. Ota, K. & Kinjo, R. Inorganic Benzene Valence Isomers. *Chem. Asian J.* **15**, 2558–2574 (2020).
2. Stock, A. & Pohland, E. Borwasserstoffe, IX.: $B_3N_3H_6$. *Ber. Dtsch. Chem. Ges.* **59**, 2215–2223 (1926).
3. Kneissl, M., Seong, T.-Y., Han, J. & Amano, H. The emergence and prospects of deep-ultraviolet light-emitting diode technologies. *Nat. Photonics* **13**, 233–244 (2019).
4. Watanabe, K., Taniguchi, T. & Kanda, H. Direct-bandgap properties and evidence for ultraviolet lasing of hexagonal boron nitride single crystal. *Nat. Mater.* **3**, 404–409 (2004).
5. Silly, M. G. et al. Luminescence properties of hexagonal boron nitride: Cathodoluminescence and photoluminescence spectroscopy measurements. *Phys. Rev. B* **75**, 085205 (2007).
6. Chopra, N. G. et al. Boron Nitride Nanotubes. *Science* **269**, 966–967 (1995).
7. Li, L. H. et al. Single deep ultraviolet light emission from boron nitride nanotube film. *Appl. Phys. Lett.* **97**, 141104 (2010).
8. Ota, K. & Kinjo, R. A neutral and aromatic boron-rich inorganic benzene. *Angew. Chem. Int. Ed.* **59**, 6572–6575 (2020).
9. Kinney, C. R. & Pontz, D. F. The structure of the organoboron oxides. *J. Am. Chem. Soc.* **58**, 197 (1936).
10. Wiberg, E. & Sturm, W. Notizen: Über Derivate eines „Borsulfols" $B_3H_3S_3$. II. Zur Kenntnis einer trimeren Metathioborsäure $[B(SH)S]_3$. *Z. Naturforsch. B* **8**, 530–531 (1953).
11. Schmidt, M. & Kiewert, E. Notizen: Zur Kenntnis des ersten Vertreters eines „Borselenol"-Systems/Triphenylboroselenol—the first representative of the "Boroselenol"-system. *Z. Naturforsch. B* **26**, 613 (1971).
12. Dias, H. V. R. & Power, P. P. Synthesis and X-ray structure of $(2,4,6\text{-}Me_3C_6H_2BPC_6H_{11})_3$: a boron-phosphorus analogue of borazine. *Angew. Chem. Int. Ed.* **26**, 1270–1271 (1987).
13. Gates, D. P., Ziembinski, R., Manners, I., Rheingold, A. L. & Haggerty, B. S. Synthesis and structure of the first hybrid borazine—phosphazene ring. *Angew. Chem. Int. Ed.* **33**, 2277–2279 (1994).
14. Hope, H., Pestana, D. C. & Power, P. P. Synthesis and structure of the novel Ga_3P_3 ring compound $[(2,4,6\text{-}Ph_3C_6H_2)GaP(cyclo\text{-}C_6H_{11})]_3$. *Angew. Chem. Int. Ed.* **30**, 691–693 (1991).
15. Waggoner, K. M., Hope, H. & Power, P. P. Synthesis and structure of $[MeAlN(2,6\text{-}iPr_2C_6H_3)]_3$: an aluminum-nitrogen analogue of borazine. *Angew. Chem. Int. Ed.* **27**, 1699–1700 (1988).
16. Wehmschulte, R. J. & Power, P. P. Reactions of $(H_2AlMes^*)_2$ (Mes* = 2,4,6-$(t\text{-}Bu)_3C_6H_2$) with H_2EAr (E = N, P, or As; Ar = aryl): characterization of the ring compounds $(Mes^*AlNPh)_2$ and $(Mes^*AlEPh)_3$ (E = P or As). *J. Am. Chem. Soc.* **118**, 791–797 (1996).
17. Seitz, A. E. et al. Pnictogen–silicon analogues of benzene. *J. Am. Chem. Soc.* **138**, 10433–10436 (2016).
18. Bartlett, R. A. & Power, P. P. Synthesis and structural characterization of the cyclic species $[GeN(2,6\text{-}i\text{-}Pr_2C_6H_3)]_3$: the first "Germanazene". *J. Am. Chem. Soc.* **112**, 3660–3662 (1990).
19. Meng, G. et al. High-efficiency and stable short-delayed fluorescence emitters with hybrid long- and short-range charge-transfer excitations. *Nat. Commun.* **14**, 2394 (2023).
20. Borden, W. T. Can a square or effectively square singlet be the ground state of cyclobutadiene? *J. Am. Chem. Soc.* **97**, 5968–5970 (1975).
21. Kollmar, H. & Staemmler, V. Violation of Hund's rule by spin polarization in molecules. *Theor. Chim. Acta* **48**, 223–239 (1978).
22. Leupin, W. & Wirz, J. Low-lying electronically excited states of cycl[3.3.3]azine, a bridged 12π-perimeter. *J. Am. Chem. Soc.* **102**, 6068–6075 (1980).
23. de Silva, P. Inverted singlet–triplet gaps and their relevance to thermally activated delayed fluorescence. *J. Phys. Chem. Lett.* **10**, 5674–5679 (2019).
24. Ehrmaier, J. et al. Singlet–triplet inversion in heptazine and in polymeric carbon nitrides. *J. Phys. Chem. A* **123**, 8099–8108 (2019).

25. Aizawa, N. et al. Delayed fluorescence from inverted singlet and triplet excited states. *Nature* **609**, 502–506 (2022).
26. Li, J. et al. Down-conversion-induced delayed fluorescence via an inverted singlet-triplet channel. *Dyes Pigments* **203**, 110366 (2022).
27. Okumura, R. et al. Development of an organic emitter exhibiting reverse intersystem crossing faster than intersystem crossing. *Angew. Chem. Int. Ed.* **63**, e202409670 (2024).
28. Kusakabe, Y., Shizu, K., Tanaka, H., Tanaka, K. & Kaji, H. An inverted singlet-triplet excited state in a pentaazaphenalene derivative (5AP-N(C12)$_2$). *Appl. Phys. Express* **17**, 061001 (2024).
29. Bedogni, M., Giavazzi, D., Di Maiolo, F. & Painelli, A. Shining light on inverted singlet-triplet emitters. *J. Chem. Theory Comput.* **20**, 902–913 (2024).
30. Ricci, G., San-Fabián, E., Olivier, Y. & Sancho-García, J. C. Singlet-triplet excited-state inversion in heptazine and related molecules: assessment of TD-DFT and ab initio methods. *ChemPhysChem* **22**, 553–560 (2021).
31. Loos, P.-F., Lipparini, F. & Jacquemin, D. Heptazine, cyclazine, and related compounds: chemically-accurate estimates of the inverted singlet-triplet gap. *J. Phys. Chem. Lett.* **14**, 11069–11075 (2023).
32. Pérez-Jiménez, ÁJ., Olivier, Y. & Sancho-García, J. C. The role of theoretical calculations for INVEST systems: complementarity between theory and experiments and rationalization of the results. *Adv. Opt. Mater.* **13**, 2403199 (2025).
33. Sobolewski, A. L. & Domcke, W. Excited-state singlet-triplet inversion in hexagonal aromatic and heteroaromatic compounds. *Phys. Chem. Chem. Phys.* **25**, 21875–21882 (2023).
34. Pershin, A. et al. Highly emissive excitons with reduced exchange energy in thermally activated delayed fluorescent molecules. *Nat. Commun.* **10**, 597 (2019).
35. Hall, D. et al. Improving processability and efficiency of resonant TADF emitters: a design strategy. *Adv. Opt. Mater.* **8**, 1901627 (2020).
36. Hall, D. et al. Modeling of multiresonant thermally activated delayed fluorescence emitters—properly accounting for electron correlation is key!. *J. Chem. Theory Comput.* **18**, 4903–4918 (2022).
37. Sanz-Rodrigo, J., Ricci, G., Olivier, Y. & Sancho-García, J. C. Negative singlet–triplet excitation energy gap in triangle-shaped molecular emitters for efficient triplet harvesting. *J. Phys. Chem. A* **125**, 513–522 (2021).
38. Valverde, D. et al. Computational investigations of the detailed mechanism of reverse intersystem crossing in inverted singlet-triplet gap molecules. *ACS Appl. Mater. Interfaces* **16**, 66991–67001 (2024).
39. de Thieulloy, L., de Sousa, L. E. & de Silva, P. Enhancing triplet harvesting in inverted singlet-triplet gap molecules through mechanistic understanding. *J. Mater. Chem. C* **13**, 16489–16498 (2025).
40. Shizu, K. & Kaji, H. Theoretical determination of rate constants from excited states: application to benzophenone. *J. Phys. Chem. A* **125**, 9000–9010 (2021).
41. Shizu, K. & Kaji, H. Quantitative prediction of rate constants and its application to organic emitters. *Nat. Commun.* **15**, 4723 (2024).
42. Povie, G., Segawa, Y., Nishihara, T., Miyauchi, Y. & Itami, K. Synthesis of a carbon nanobelt. *Science* **356**, 172–175 (2017).
43. Xia, J. & Jasti, R. Synthesis, characterization, and crystal structure of [6]cycloparaphenylene. *Angew. Chem. Int. Ed.* **51**, 2474–2476 (2012).
44. Xue, J. Y. et al. Cyclo-*meta*-phenylene revisited: nickel-mediated synthesis, molecular structures, and device applications. *J. Org. Chem.* **79**, 9735–9739 (2014).
45. Stéphan, O. et al. Formation of small single-layer and nested BN cages under electron irradiation of nanotubes and bulk material. *Appl. Phys. A* **67**, 107–111 (1998).
46. Golberg, D., Bando, Y., Stéphan, O. & Kurashima, K. Octahedral boron nitride fullerenes formed by electron beam irradiation. *Appl. Phys. Lett.* **73**, 2441–2443 (1998).
47. Oku, T., Nishiwaki, A., Narita, I. & Gonda, M. Formation and structure of $B_{24}N_{24}$ clusters. *Chem. Phys. Lett.* **380**, 620–623 (2003).
48. Matsunaga, N., Cundari, T. R., Schmidt, M. W. & Gordon, M. S. A comparative study of the bonding in heteroatom analogues of benzene. *Theor. Chim. Acta* **83**, 57–68 (1992).
49. Matsunaga, N. & Gordon, M. S. Stabilities and energetics of inorganic benzene isomers: prismanes. *J. Am. Chem. Soc.* **116**, 11407–11419 (1994).
50. Amano, H., Kito, M., Hiramatsu, K. & Akasaki, I. P-type conduction in Mg-doped GaN treated with low-energy electron beam irradiation (LEEBI). *Jpn. J. Appl. Phys.* **28**, L2112 (1989).
51. Nakamura, S., Mukai, T. & Senoh, M. Candela-class high-brightness InGaN/AlGaN double-heterostructure blue-light-emitting diodes. *Appl. Phys. Lett.* **64**, 1687–1689 (1994).
52. Nakamura, S. & Krames, M. R. History of gallium–nitride-based light-emitting diodes for illumination. *Proc. IEEE* **101**, 2211–2220 (2013).
53. Akasaki, I. Nobel Lecture: Fascinated journeys into blue light. *Rev. Mod. Phys.* **87**, 1119–1131 (2015).
54. Frisch, M. J. et al. Gaussian 16 Rev. C.01. (2016).
55. TURBOMOLE V7.4.1 2019, a development of University of Karlsruhe and Forschungszentrum Karlsruhe GmbH, 1989-2007, TURBOMOLE GmbH, since 2007. http://www.turbomole.com.
56. Domcke, W., Sobolewski, A. L. & Schlenker, C. W. Photooxidation of water with heptazine-based molecular photocatalysts: insights from spectroscopy and computational chemistry. *J. Chem. Phys.* **153**, 100902 (2020).
57. Dreuw, A. & Hoffmann, M. The inverted singlet-triplet gap: a vanishing myth? *Front. Chem*. **11**, 1239604 (2023).
58. Gao, X. et al. Evaluation of spin-orbit couplings with linear-response time-dependent density functional methods. *J. Chem. Theory Comput.* **13**, 515–524 (2017).

Acknowledgements

The quantum chemical calculations using the Gaussian 16 and Turbomole program packages were performed on the SuperComputer System, Institute for Chemical Research, Kyoto University. This work was also supported by JSPS KAKENHI: Grant-in-Aid for Transformative Research Areas (A), "Photokineticism" (Grant Numbers JP26H00371 and JP26H00372), Grant-in-Aid for Scientific Research (A) (Grant Number JP26H02293), JST SPRING (JPMJSP2110), JSPS Core-to-Core Program (Grant Number JPJSCCA20220004), and JST CREST (Grant Number JPMJCR2431).

Author contributions

H.K. supervised the project. Theoretical calculations were mainly performed by K.S. and partly by K.I. and H.U. All authors contributed to the writing of this paper and have approved the final version.

Competing interests

The authors declare no competing interests.

Additional information

Supplementary information The online version contains supplementary material available at https://doi.org/10.1038/s42004-026-02141-0.

Correspondence and requests for materials should be addressed to Hironori Kaji.

Peer review information *Communications Chemistry* thanks the anonymous reviewers for their contribution to the peer review of this work. A peer review file is available.

Reprints and permissions information is available at http://www.nature.com/reprints

Publisher's note Springer Nature remains neutral with regard to jurisdictional claims in published maps and institutional affiliations.

Open Access This article is licensed under a Creative Commons Attribution 4.0 International License, which permits use, sharing, adaptation, distribution and reproduction in any medium or format, as long as you give appropriate credit to the original author(s) and the source, provide a link to the Creative Commons licence, and indicate if changes were made. The images or other third party material in this article are included in the article's Creative Commons licence, unless indicated otherwise in a credit line to the material. If material is not included in the article's Creative Commons licence and your intended use is not permitted by statutory regulation or exceeds the permitted use, you will need to obtain permission directly from the copyright holder. To view a copy of this licence, visit http://creativecommons.org/licenses/by/4.0/.

© The Author(s) 2026